Process Setup and Boundaries of Wire Electron Beam Additive Manufacturing of High Strength Aluminum Bronze

J. Raute *, M. Biegler , M. Rethmeier

Posted Date: 27 June 2023

doi: 10.20944/preprints202306.1925.v1

Keywords: wire electron beam additive manufacturing; aluminum bronze; wire-based additive manufacturing; EBAM; DED-EB

Article

Process setup and boundaries of Wire Electron Beam Additive Manufacturing of high strength aluminum bronze

J. Raute[1]*, M. Biegler[2] and M. Rethmeier[3,1,2]

[1] Fraunhofer Institute for Production Systems and Design Technology (IPK), Pascalstraße 8-9, 10587 Berlin, Germany;
[2] Bundesanstalt für Materialforschung und -prüfung (BAM), Unter den Eichen 87, 12205 Berlin, Germany;
[3] Technische Universität Berlin, Straße des 17. Juni 135, 10623 Berlin, Germany;
* Correspondence: julius.raute@ipk.fraunhofer.de

Abstract: In recent years, in addition to the commonly known wire-based processes of Directed Energy Deposition using lasers, a process variant using the electron beam has also developed to industrial market maturity. The process offers particular potential for processing highly conductive, reflective or oxidation-prone materials. However, for industrial usage there is a lack of comprehensive data on performance, process limits and possible applications. The present study deals with this problem using the example of the high-strength aluminum bronze CuAl8Ni6. Multi-stage test welds are used to determine the physically possible process limits and draw conclusions about the suitability of the parameters for additive manufacturing. For this purpose, optimal ranges for energy input, possible welding speeds and the scalability of the process were investigated. Finally, additive test specimens in the form of cylinders and walls are produced and the hardness profile, microstructure and mechanical properties are investigated. It is found that the material CuAl8Ni6 can be well processed by wire electron beam additive manufacturing. The microstructure is similar to a cast structure, the hardness profile over the height of the specimens is constant and the tensile strength and elongation at fracture values achieved correspond to the specification of the raw material.

Keywords: wire electron beam additive manufacturing; aluminum bronze; wire-based additive manufacturing; EBAM; DED-EB

1. Introduction

At the current state of the art, additive manufacturing of copper alloys is possible using various processes. In this context, processes based on powder bed fusion using lasers as a heat source (PBF-LB) have been extensively investigated, which proved to be particularly advantageous for the production of complex components made of pure copper [1] but also of conventional bronzes [2]. Since pure copper and low alloy Cu materials almost completely reflect laser radiation in the infrared as well as near infrared range due to their physical properties, various workarounds had to be developed [3]. Usually, green [4] or blue [5] lasers are used to increase the absorption coefficient, or beam pulsing is performed in combination with high powers.

Compared to PBF-LB, laser-based Directed Energy Deposition (DED-LB) processes enable significantly higher deposition rates in the processing of copper alloys [6]. However, since the material is fed in powder or wire form via a nozzle, only certain alloys can be used without restrictions due to the previously mentioned problem of reflection. Thus, with common solid-state lasers, adapted process control is possible for various bronzes in powder form [7], since the increased surface area and

 doi:10.20944/preprints202306.1925.v1

alloying of other elements improve the absorption behavior [8]. The study by Siva et al. shows that low-alloy copper can be processed with laser powder DED using a green laser. However, only a small part of the laser power used is actually available to the process due to reflections and high thermal conductivity, which means that only rather low working speeds are possible [4].

Arc-based DED processes (DED-Arc), often referred to as wire arc additive manufacturing, have also been tested for application to Cu alloys. As the work of Wang et al. shows using the example of a Cu-Al bronze, processing is possible in principle [9]. However, in the case of aluminum bronze, an anisotropy of mechanical properties is shown compared to other processes [10]. Similar observations were made by Guo et al. for the application to Cu-Ni alloys, where the strength values were found to be good overall [11]. However, in some cases significant limitations are shown with regard to the quality and achievable accuracy of the fabricated structures [12].

The above-mentioned difficulties in the processing of copper can be overcome by using the electron beam as a heat source [13]. This is evident from work in the field of Electron Beam Powder Bed Fusion (PBF-EB) [14]. In particular, when applied to low-alloy Cu materials or pure copper, PBF-EB can convince by high component qualities with simultaneously high electrical conductivity, as demonstrated by the study of Megahed et al. [15].

A process which combines the advantages of the electron beam for the processing of Cu with higher deposition rates is the DED-EB. In this process, a wire-shaped filler material is melted inside a vacuum chamber by a focused electron beam. A schematic illustration of the process is shown in Figure 1. The beam is usually stationary during the welding process, while the welding feed is realized by moving the component on CNC-controlled work tables or fixtures. Due to the characteristics of the beam source, the wire feed is usually lateral to the beam direction. Therefore, rotating fixtures are often used to overcome the directionality of the manipulation, e.g. for rotation-symmetrical components [16]. Here, the electron beam creates a melt pool on the surface of the component or substrate as well as on the wire tip itself. By slightly offsetting the intersection between the electron beam and wire axis and the surface of the component, a stable bridge of molten material is obtained. The continuous movement of the table thus allows the production of two-dimensional coatings and three-dimensional components. In DED-EB, in line with other AM or coating technologies, energy input [17], hardness [16], dilution or bonding, and favorable track geometry are usually considered as essential quality characteristics for the suitability of a parameter set for additive buildup [18].

The process has been investigated in the past primarily for use on reactive materials, such as titanium alloys, due to the excellent protection against oxidation within the working vacuum [18]. However, studies have also been carried out in the field of steel materials [17] as well as corrosion-resistant nickel-based alloys [19]. As far as the practical application of components manufactured by means of DED-EB is considered, initial findings have already been made on various materials. For example, in the work of Baufeld et al. it was shown for the stainless steel 316L that the tensile strengths achievable by DED-EB are approximately at the base material level [20]. Recent studies also demonstrate the good workability of Cu wires for large-volume rotating parts using the example of a rocket engine [21]. The potential of DED-EB has also been illustrated in the field of aluminum bronze by initial test series. The work of Khoroshko et al. uses the case of a single-phase Cu-Al alloy to investigate the microstructure achieved as well as mechanical characteristics on the basis of tensile and compression tests [22]. This showed a pronounced anisotropy in the microstructure, which also manifested itself in the mechanical properties of the samples. Recent investigations by Zykova et al. on the alloy CuAl9Mn2 confirm this behavior [23]. In particular, the control of energy input is of special importance in DED-EB in order to favor the formation of advantageous microstructures and to exploit the potential of high-strength aluminum bronzes. The anisotropic distribution of material properties and microstructure, which requires a profound understanding of the process for further optimization, proved to be particularly problematic.

2. Materials and Methods

Preprints (www.preprints.org) | NOT PEER-REVIEWED | Posted: 27 June 2023 doi:10.20944/preprints202306.1925.v1

2.1. Experimental setup

The experiments were carried out on an EBG15-150 K30 electron beam system from pro-beam GmbH & Co. KGaA, which was equipped with a DIX WDE 515 wire feeding device from Dinse GmbH. A constant accelerating voltage of 120 kV was set for all experiments. The operating vacuum during the welding process was between 0.5·10-4 mbar - 1·10-3 mbar. The experimental setup is shown in Figure 1. The alignment between the wire feeder, electron beam and substrate is critical to the process [17]. The optimal settings for this were determined empirically in preliminary experiments and kept constant. The angle of inclination α of the wire conveyor was 30° with a distance of the wire tip to the surface H of 4.3 mm. The intersection point between the wire axis and the electron beam is referred to as the working point, which had an offset from the substrate surface h of 2 mm. The working distance between the deflection coil and the working point was 880 mm. As welding figure concentric circles with an amplitude in X as well as Y direction of 2 mm - 4 mm, depending on the parameter set, were used in the surface focus of the workpiece.

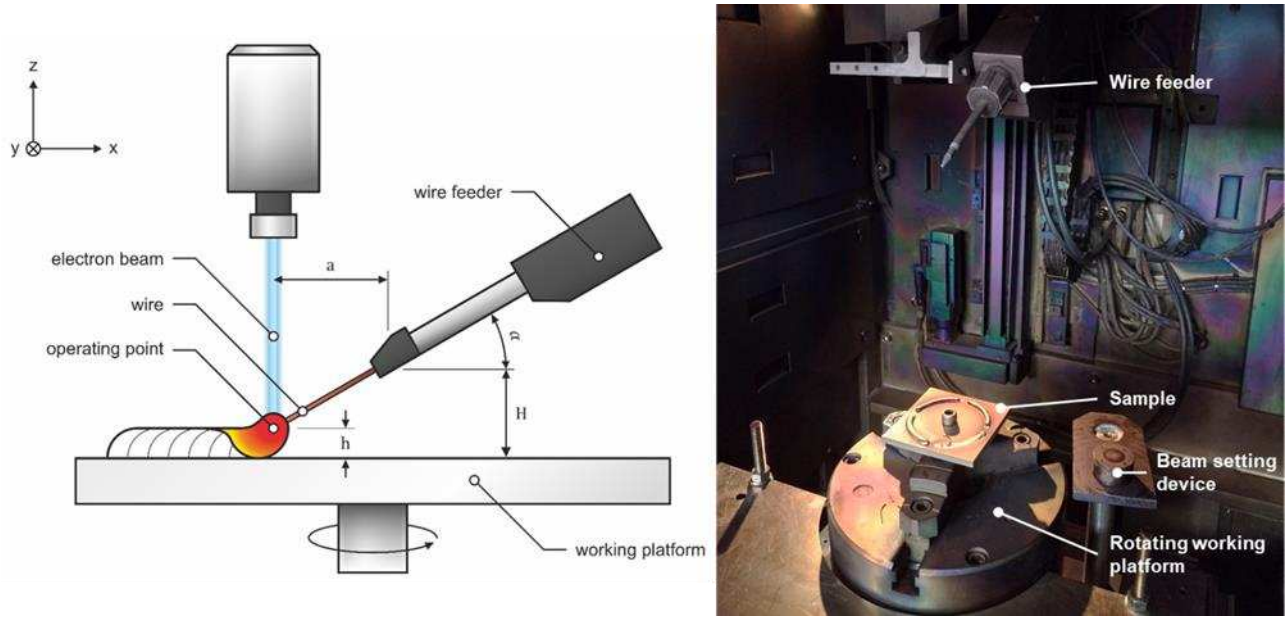

Figure 1. Experimental setup.

As substrate material for the welding tests, square plates of the material 1.4404 with a side length of 100 mm and a thickness of 6 mm were used. Test welds were performed on these in form of circular sections with a diameter of 40 mm and a size of the circular section of 35° for preliminary tests and in form of cylinders and walls for additive welding tests. The experiments were carried out with a filler wire made of CuAl8Ni6 and a diameter of 1.0 mm. The chemical composition of the alloy is shown in Table 1.

Table 1. Chemical composition of the materials.

Substrate material: X2CrNiMo17-12-2 (1.4404)							
Element	**Fe**	**Cr**	**Ni**	**Mo**	**Mn**	**Si**	**C**
Amount / Ma%	Bal.	17.41	10.1	1.97	1.58	0.36	0.03

Welding wire: CuAl8Ni6					
Element	**Cu**	**Al**	**Ni**	**Fe**	**Mn**
Amount / Ma%	Bal.	9.0	4.5	3.5	1.3

Preprints (www.preprints.org) | NOT PEER-REVIEWED | Posted: 27 June 2023 doi:10.20944/preprints202306.1925.v1

2.2. Experimental procedure and process parameters

2.2.1. Tests on energy input

Initially, the process limits for the material were determined. In particular, the optimum energy input had to be identified. This was done on the basis of 9 test welds with different welding parameters. An overview of the parameters used is shown in Table 2. Subsequently, the track geometry and the wetting angle were measured optically by means of focus variation using the Alicona InfiniteFocus measuring system to evaluate the deposition quality. All target values at the cross sections can be seen in Figure 2.

2.2.2. Tests on welding speed and dilution

In the second step, the influence of the welding speed on the process is examined. In particular, it was investigated whether this has an influence on the dilution between the base material and the filler material at constant energy input. The volumetric energy was defined based on the findings of the previously conducted tests. A constant wire feed rate of 3.5 m/min and a constant volumetric energy of 23.6 J/mm³ are set, while the welding speed increases track by track. For this purpose, 4 test tracks for each of the two alloys are welded, cut up for evaluation by means of wet cut-off grinders and prepared to form metallographic cross-sections of the weld. Afterwards the dilution is measured using the ImageJ software.

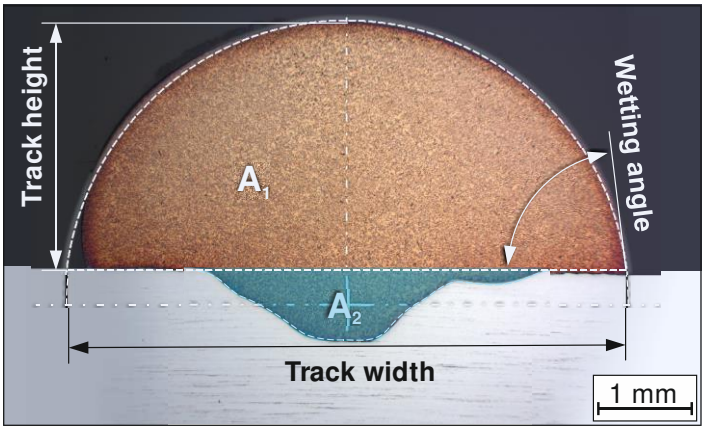

$$Dilution = \frac{A_2}{A_1 + A_2} \cdot 100\%$$

Figure 2. Target values at the track geometry.

2.2.3. Test on scalability

After determining suitable values for energy input and welding speed, the scalability of the process is investigated by changing the beam current and the wire feed rate. The tests are carried out on 4 test welds. The energy input is set constant at 23.6 J/mm³ and the welding speed is adjusted to 6 mm/s. The beam current and wire feed rate are incrementally increased by the same factor. The track width and track height are then measured on a polished cross-section of the specimens using a digital microscope, and hardness measurements are carried out. The average of at least four evenly distributed hardness measurement points per sample are used for further evaluation. The hardness measurement is carried out according to Vickers in the small load range with HV1.

2.2.4. Hardness profile measurements and microstructure

The additive test specimens for the evaluation of microstructure and hardness are manufactured in the form of cylinders with a diameter of 80 mm and a height of 20 mm. The wall thickness is achieved here exclusively via the width of a single track. Again, the constant volume energy approach

 doi:10.20944/preprints202306.1925.v1

is followed and the values determined at the beginning are considered as the basis for the combination of beam current and wire feed. Two cylinders are manufactured with different parameter sets. The parameter combinations are selected in such a way that one variant each lies at the lower end of the stable process range and at the upper end. This is intended to demonstrate the possibilities of the DED-EB on the existing equipment for the production of fine structures with low deposition rates as well as large structures with high deposition rates. In order to evaluate microstructure and possible defects, a part of the wall of each of the additively manufactured test cylinders Z1 and Z2 is taken over the entire height of the cylinder and a cross section is made. The hardness profile is measured along a line starting from the top of the specimens into the material of the substrate plate. The measurement is carried out according to the Vickers method in the HV1 variant. The spacing of the measuring points is selected according to the recommendations of ISO 6507 for the selected test method, under the assumption of ductile material behavior.

2.2.5. Tensile testing

In order to produce the tensile specimens, walls are built up. The wall thickness corresponds to the width of a single track. The walls are built up analogously to the cylinders in a unidirectional process. For each material, 3 identical specimen walls are set up to ensure statistical validation of the results. As a guideline value for the height, 20 mm is specified to ensure sufficient room for subsequent machining. The optimum range for the volume energy in the preliminary tests and a constant welding speed are used as the basis for parameter selection. The tensile specimens were cut horizontally from the additively built walls by means of machining on a CNC machining center under cooling. The geometry of the specimens corresponds to a flat tensile specimen of the variant E2 x 6 x 20 according to DIN 50125. The tensile test is performed using method A with a strain-controlled test speed. Here, the output signal of the extensometer is used for control. Tensile strength, elongation at break and the stress-strain curves are thus determined via the evaluation software of the testing machine. The test is carried out at room temperature until total fracture.

Table 2. Overview process parameters.

Sample No.	Beam current / mA	Welding speed / mm/s	Wire feed / m/min	Volume energy / J/mm³	Experimental purpose
1	9	4	3.5	23.6	Tests on energy input
2	12	4	6	18.3	
3	12	4	1	110	
4	6	4	6	9.2	
5	9	4	6	13.8	
6	12	4	3.5	31.4	
7	6	4	3.5	15.7	
8	9	4	1	82.5	
9	6	4	1	55	
10	9	3	3.5	23.6	Tests on welding speed and dilution
11	9	3.6	3.5	23.6	
12	9	4.5	3.5	23.6	
13	9	6	3.5	23.6	
14	4.5	6	1.75	23.6	Test on scalability
15	9	6	3.5	23.6	
16	13.5	6	5.25	23.6	
17	18	6	7	23.6	
Z1	4.5	6	1.75	23.6	Hardness profile measurements
Z2	18	6	7	23.6	

W1; W2; W3	13.5	6	5.25	23.6	Tensile testing

3. Results and discussion

3.1. Tests on energy input

The deposited test tracks were welded with different energy inputs and evaluated optically. At a volumetric energy of 15.7 J/mm³, as in parameter set no. 7, wire movement disturbances occur more frequently, leading to a process termination. If the volume energy is lowered further, as in parameter set No. 4, the energy supplied is no longer sufficient to melt the wire completely. The two test points are therefore not considered for further evaluation. The wetting angle is used as a parameter for estimating the suitability of the welded tracks within the stable process range for additive manufacturing. This provides conclusions about the wetting behavior of the melt on the surface of the substrate. Too low wetting angles < 45° indicate a strong flow of the molten wire, while excessively large values > 90° suggest insufficient wetting or bonding. Figure 3 D) shows the change in wetting angle with increasing volumetric energy. Satisfactory track qualities, with respect to the wetting behavior, are shown in the range of 18.3 J/mm³ to 31.4 J/mm³. Higher energy inputs into the volume of the melt caused a rapid reduction of the wetting angle due to strong flow of the deposited material and are therefore considered unsuitable for additive manufacturing.

3.2. Tests on welding speed and dilution

The relationship between welding speed and dilution can be seen in Figure 3 C). It shows a trend towards increasing dilution with higher welding speed. The stability of the material transition from the wire tip to the substrate may be used as an explanation. For constant values of beam current and wire feed, increasing the welding speed causes the same amount of molten material to be spread over a longer section, making the transition of melted material between the wire end and the substrate more unstable. This might cause the electron beam at constant power to penetrate deeper into the base material during phases of temporarily reduced deposition rate.

In the literature on DED-EB, the relationship between beam current and dilution is already known [18]. Nevertheless, the welding speed is mostly neglected as an influencing variable, since the beam current is often considered as the main factor for controlling the dilution. This approach has some disadvantages in the process design. If, for example, the method of a constant volume energy is used to ensure specific microstructures or mechanical properties, the value of the beam current is fixed to the amount of wire feed and can only be varied within small limits to set desired values of the dilution. If a certain degree of dilution is required due to technological specifications, this can only be achieved by adjusting the welding speed. In the literature, the dilution of DED-EB has already been investigated for other materials. For low-alloy steels [17] or titanium materials [18], minimum values of approx. 17 % and 28 %, respectively, were found. However, the measured dilutions in the present work for aluminum bronze were significantly lower at values of approx. 4 % - 12 %.

3.3. Test on scalability

After suitable ranges for volume energy and welding speed have been determined, the next step is to test the scalability of the process in order to ensure individual influencing of the track geometry while maintaining the same component properties for the additive buildup. For this purpose, the parameters wire feed and beam current were increased stepwise by the same factor, while welding speed and volume energy remained constant. An overview of the development of the track geometry with stepwise increase of the deposition rate is shown in Figure 5 on the cross sections of the samples. Deposition rates of 0.6 kg/h - 2.5 kg/h can be realized for the alloy CuAl8Ni6. In the literature, deposition rates for comparable Cu alloys at DED-EB are about 1.9 kg/h and thus within the investigated range [20]. For pure copper and low-alloy copper materials, Baufeld et al. achieved values for the DED-EB of 1.5 kg/h to 3.3 kg/h, although the higher density of the material must be taken into account

Preprints (www.preprints.org) | NOT PEER-REVIEWED | Posted: 27 June 2023 doi:10.20944/preprints202306.1925.v1

here [21]. In order to obtain a rough estimation of the influence of the scaling on mechanical parameters, hardness measurements are carried out. The result of these measurements as well as the development of the track geometry are shown in the form of diagrams in Figure 3 A) and in relation to wire feed and beam current. There is a slight decrease in hardness with gradual increase in beam current and wire feed. The hardness values achieved above 200 HV1 are within a normal range for the material. They thus correspond to qualities achievable by other AM processes for Al bronzes, such as DED-Arc [12]. The course of the hardness is relatively constant over the increase in beam current and wire feed. Only the hardness value of the lowest setting is slightly above the other samples.

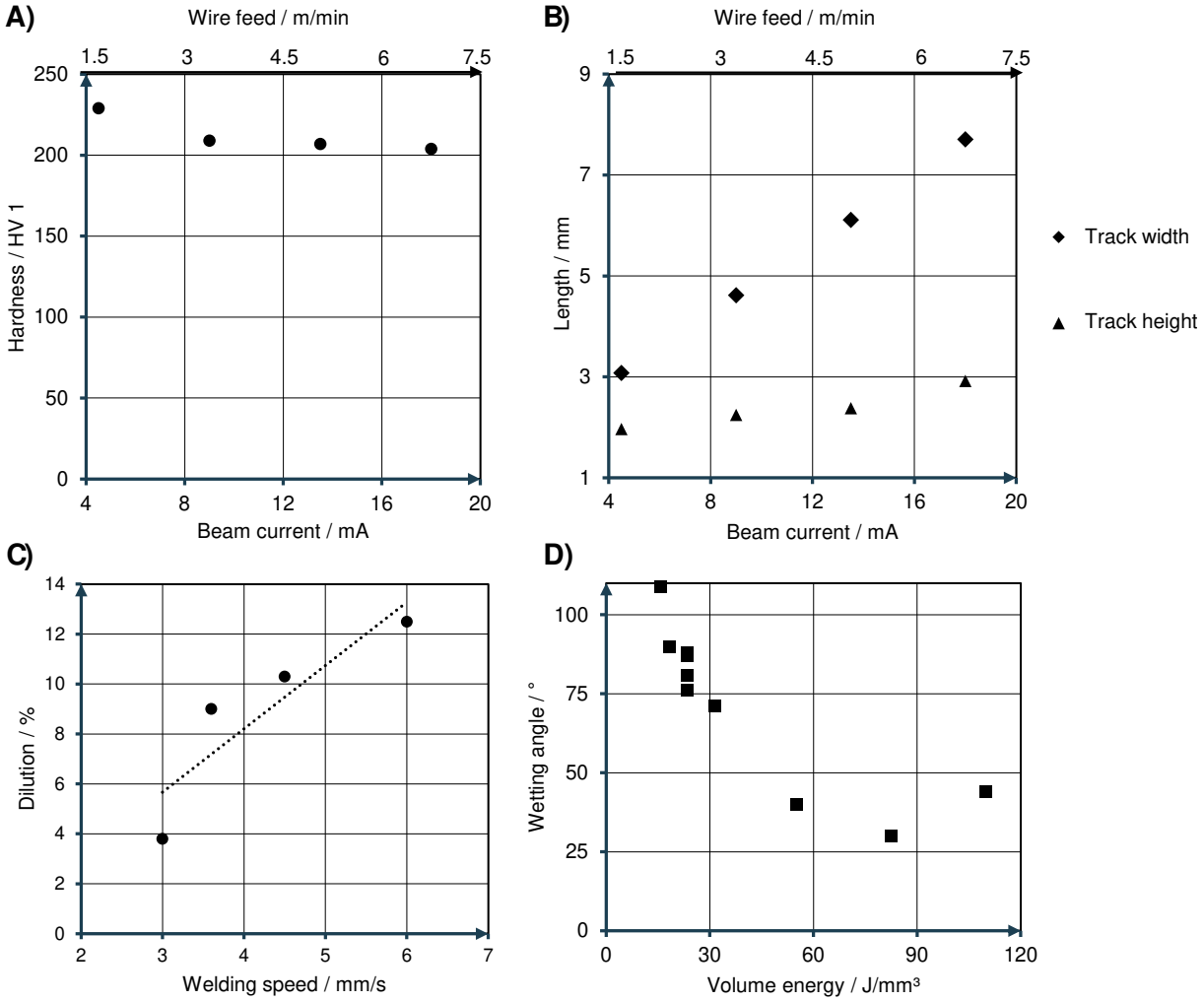

Figure 3. (**A**) Hardness over scaling; (**B**) Development of track geometry over scaling; (**C**) Dilution over welding speed; (**D**) Dependence of the wetting angle on the volumetric energy.

Figure 3 B) shows the change in track width and track height when the process is scaled. In addition to the measured values, Figure 4 shows the evolution of the track geometry on cross sections. The curves clearly show that the track width increases significantly faster than the track height when the beam current and wire feed rate are increased stepwise. The plots are nearly linear, indicating good scalability and stability of the process in the identified parameter range. The present results on the scaling of the process at constant volumetric energy based on wire feed and beam current confirm the behavior known for mild steel in the case of DED-EB, as observed by Fuchs et al. [17]. There, a significantly stronger increase of the track width compared to the height was shown, too.

Preprints (www.preprints.org) | NOT PEER-REVIEWED | Posted: 27 June 2023 doi:10.20944/preprints202306.1925.v1

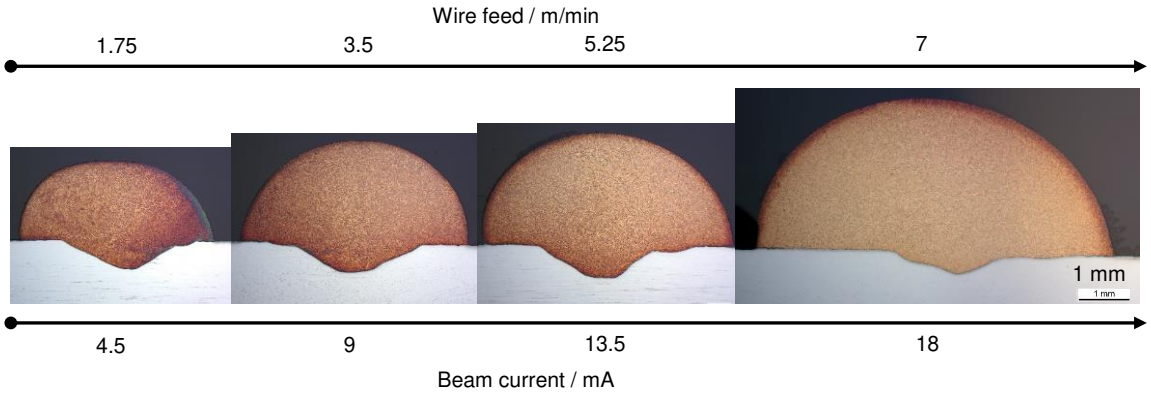

Figure 4. Development of track geometry when scaling the process via wire feed and beam current.

3.4. Microstructure

The use of a rotating clamping system for the production of the cylinders, proved to be favorable for a homogeneous process and to avoid internal defects. Thus, both cylinders show no pores, inclusions or cracks above the base plate. A major advantage of using a rotary table is that it compensates for the directionality of the DED-EB's single-sided wire feed. This offers the possibility to fix wire and electron beam in the optimal alignment and to work in a continuous manner. This conclusion was already formulated by the work of Kalashnikov et al. which dealt with different manufacturing strategies for titanium components at the DED-EB [16].

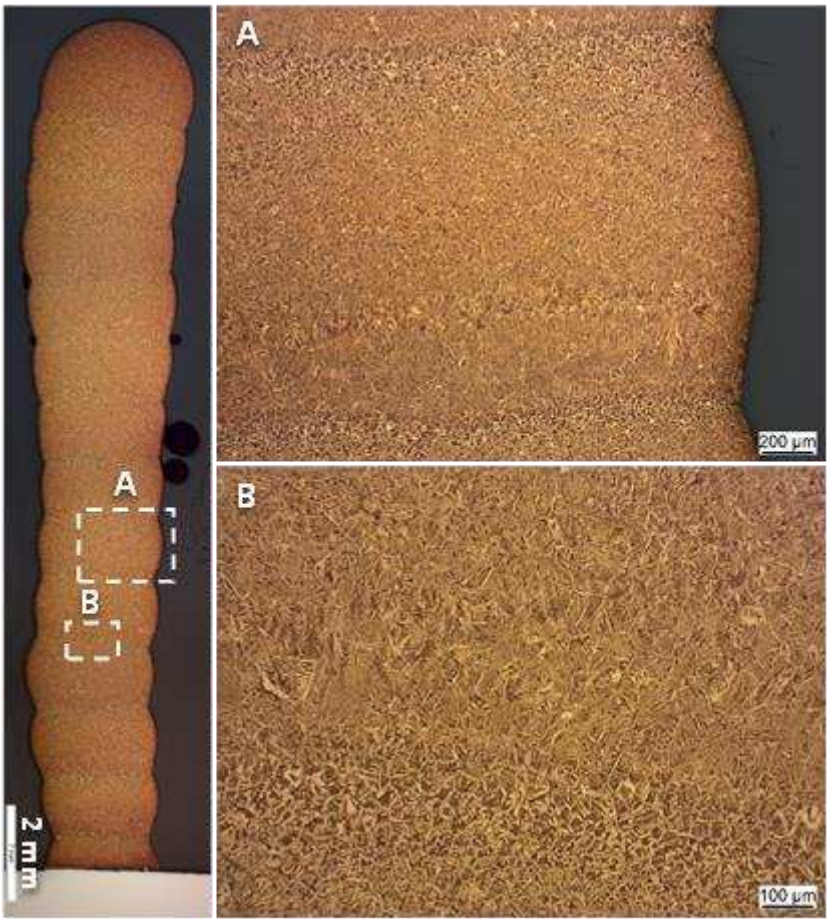

Figure 5. Microstructure of selected areas on the etched cross section of sample Z1.

 doi:10.20944/preprints202306.1925.v1

The microstructure is evaluated on the basis of images taken by a digital microscope on etched cross-sections.

Figure 5 shows the microstructure of the thin-walled cylinder Z1. The macroscopic overview image of the section shows a roughly uniform and fine-grained microstructure over the entire height of the cylinder. The individual layers can be identified on the basis of dark regions of partially re-melted material. The detailed images show a dendritic shape of the grains. Such microstructures are common in aluminum bronzes of similar composition and correspond to the microstructure of die castings. The visible bright needle-shaped grains are therefore dendritic solid solutions of Cu and Al embedded in a quasieutectoid matrix [24]. The microstructure of the thick-walled cylinder Z2 in Figure 6 is similar to the appearance of the first sample. However, the layer transitions are less sharp, due to the remelting of a larger area because of the high beam power. The microstructure also shows a finer expression of the striped dark areas around the bright Cu-Al solid solutions. This indicates a presence of additional Fe- and Ni-rich phases, so-called $\varkappa$-phases, in the quasieutectoid solid solution structure. Such microstructures are promoted in Cu-Al alloys, especially by high temperatures above 800°C in combination with slow cooling, e.g. in a furnace [8].

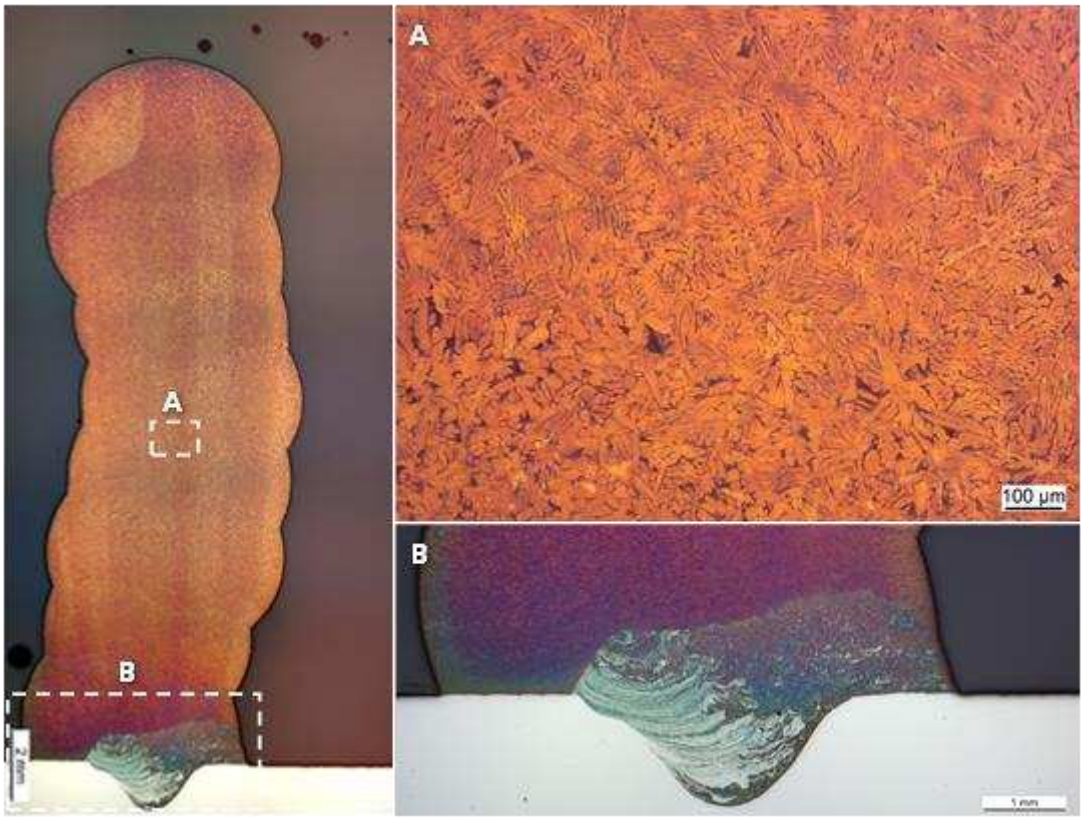

Figure 6. Microstructure of selected areas on the etched cross section of sample Z2.

The microstructure observed in the additively manufactured components is in agreement with the results of other studies on DED-EB, as long as a two-phase alloy with a correspondingly high aluminum content was used, such as in the work by Zykova et al. with the material CuAl9Mn2 [23]. In contrast, other works with lower alloyed or single-phase aluminum bronzes show a different behavior. For example, Khoroshko et al. were able to observe a significantly coarser microstructure with pronounced grain growth over the entire component height during additive manufacturing of a copper alloy with an aluminum content of 7.5% [22], which is usually known from the field of low-alloyed copper materials [21].

Preprints (www.preprints.org) | NOT PEER-REVIEWED | Posted: 27 June 2023 doi:10.20944/preprints202306.1925.v1

In the case of DED-EB, due to the vacuum, heat transfer can only take place via the fixtures as well as thermal radiation. To avoid surface oxidation, the specimens are removed from the high vacuum only after a certain cooling time. Since more heat is introduced in the case of the thick-walled cylinder, but the cooling conditions remain unchanged, the increased occurrence of such phases is plausible. In order to achieve a consistent microstructure and geometry despite changes in heat dissipation, a reduction of the energy input over the height of the components is necessary. Other works also show the necessity of adjusting the beam power during DED-EB, as already postulated by Baufeld et al. for titanium alloys [20], Fuchs et al. for steel [17], and Gurianov et al. using nickel-based materials as an example [19]. This reduction of the energy input depends on the material as well as the geometry and was empirically determined in the case of the additive test cylinders and realized by lowering the beam current. The reduction amounts to 30 % over the height of the specimens. Of this, 15 % was reduced linearly over the first 3 layers and the remaining 15 % linearly until the final height was reached. Comparable investigations on aluminum bronze in the DED-EB range reduced the beam current over the height by approx. 40 % [23].

At the base of the cylinder, a distinctive penetration into the base plate can be seen. Due to the limited possibility of mixing the two alloys, a large portion of the segregated steel is re-deposited at the bottom of the cylinder. However, the dilution is limited to a tolerable area of the first layer, which would have to be removed anyway in an additive manufacturing process when the base plate is cut off.

3.5. Hardness profile measurements

Figure 7 shows the hardness profile of specimen Z1. The plot of the graph shows slight local variations of the hardness value over the height of the cylinder wall. The measured hardnesses are in the range of approx. 160 HV1 to 210 HV1. At the lower end of the specimen, in the right area of the graph, there is a slight trend towards an increase in hardness, which can be attributed to the faster cooling and the changed heat dissipation at the beginning of the build process on the cold plate. The hardness trend over the height of the specimen is relatively uniform overall and shows no significant deviations.

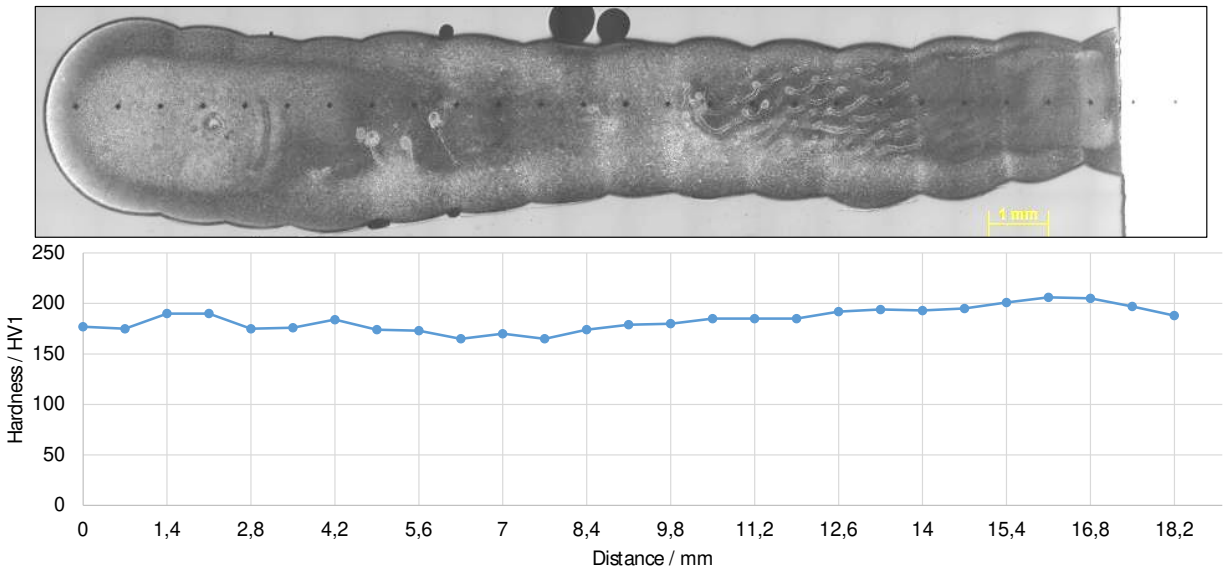

Figure 7. Hardness profile and position of measuring points sample Z1.

Figure 8 shows the hardness profile on cylinder Z2 with the maximum tested deposition rate for the material CuAl8Ni6. In this case, again, the hardness profile is almost uniform over the entire height of the cylinder. The increased hardness values at the base of the cylinder can be attributed to

Preprints (www.preprints.org) | NOT PEER-REVIEWED | Posted: 27 June 2023 doi:10.20944/preprints202306.1925.v1

the fact that measurements were already taken in the dilution area of the first layer and in the base material. In contrast to cylinder Z1 with its lower deposition rate, cylinder Z2 shows a slight decrease in the measured hardness in the range of approx. 150 HV1 to 170 HV1. However, the measured values for both specimens are within the specification of the material and are comparable with conventional aluminum bronze castings from the shipbuilding and marine engineering sector [8].

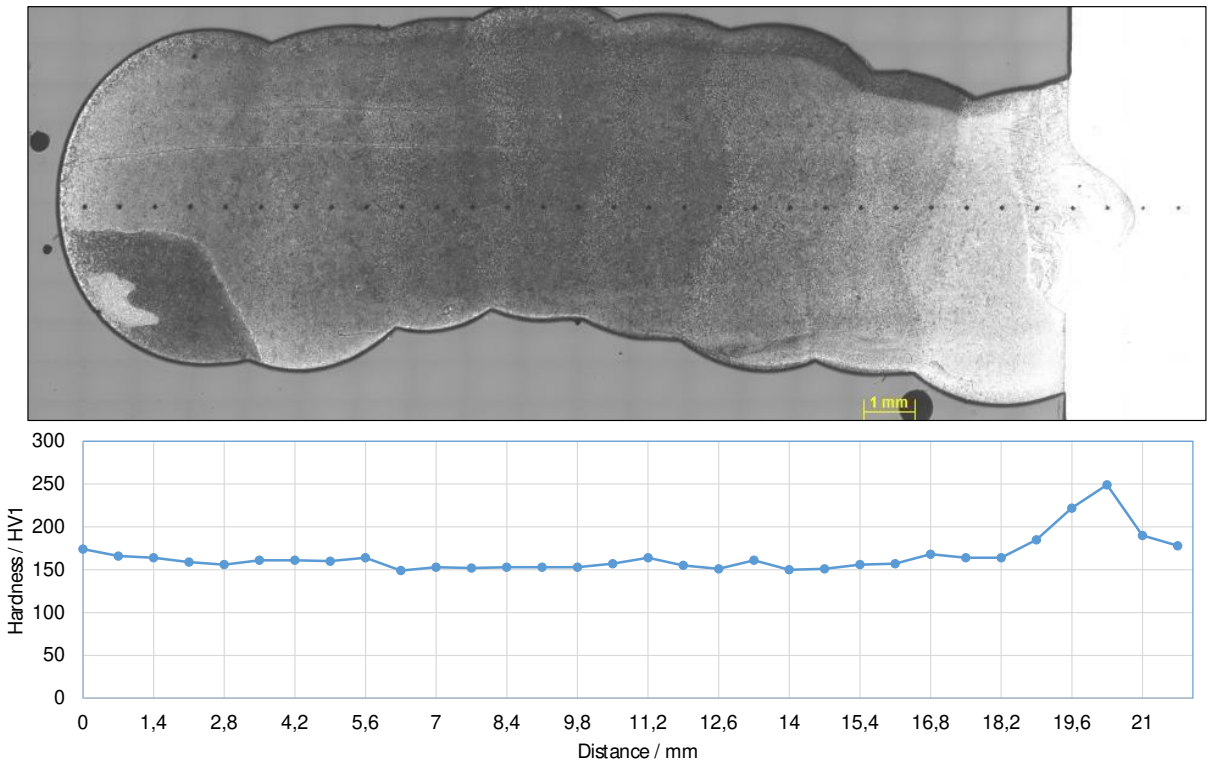

Figure 8. Hardness profile and position of measuring points sample Z2.

3.6. Tensile testing

The results of the tensile tests for yield strength, tensile strength and elongation at fracture are listed in Table 3. The graphs for the tensile tests of the individual specimens are shown in Figure 9. The evaluation of the tensile tests for the alloy CuAl8Ni6 shows average values for the yield strength of approx. 369 MPa, for the tensile strength approx. 693 MPa and an average elongation at break of 18 %. While specimens W1 and W2 show a good agreement of the material behavior, the values of specimen W3 are somewhat below the others. On average, however, the values achieved meet the material specifications of the wire manufacturer. Thus, the data sheet specifies a yield strength of approx. 380 MPa, a tensile strength of 600 MPa and an elongation at break of 16 %. In the case of specimens W1 and W2, the values for tensile strength and elongation at break are even significantly exceeded for the specimens manufactured by DED-EB. One reason for this could be the special cooling conditions of the buildup process carried out in a vacuum. In the case of the alloy used, this favors the formation of a ductile microstructure of Cu-Al solid solutions. Due to the contents of Ni and Fe, the alloy exhibits a fine microstructure despite the high heat input in the buildup process [3]. Considering the known alloy behavior, it can be assumed that the reheating in the continuous buildup process in combination with the slow cooling by the vacuum also suppress the precipitation of brittle β-phases in favor of the solid solutions and produce an accumulation of finely divided $\varkappa$-phases [8].

Table 3. Overview of the achieved mechanical properties.

 doi:10.20944/preprints202306.1925.v1

Sample No.	Yield strength / MPa	Tensile strength / MPa	Elongation at fracture / %
W1	382	710	21
W2	344	694	19.8
W3	379	675	12.4

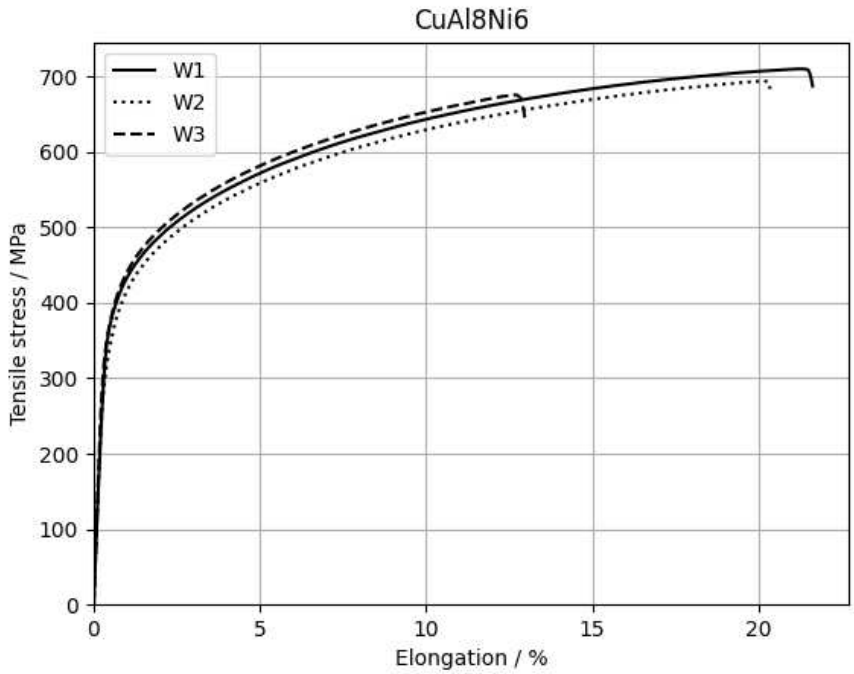

Figure 9. Results of the tensile tests.

Although this slightly decreases the hardness compared to samples with faster cooling, as shown by the comparison of the hardness profile measurement on thin-walled cylinders, tensile strength and elongation at break are improved.

The values are thus even higher than the qualities achieved for other copper materials in the DED-LB. For example, the work of Wang et al. on the copper-nickel alloy CuNi15Sn8 shows good elongations at break, but the tensile strengths achieved of approx. 327 MPa are significantly below the expected values of the material, which reach approx. 500 MPa for usual semi-finished products in strip form [6]. A similar behavior is also seen in the DED-Arc process, as suggested by the study of Chen et al. There, the material CuAl8Ni2 also showed a pronounced grain growth over the height of the additively manufactured samples as well as a lower tensile strength compared to the expected values of conventional manufacturing processes [10].

For a more detailed assessment of the results, the work of Khoroshko et al. can be consulted [22]. There, the mechanical properties of a Cu-Al alloy with 7.5 % aluminum processed by DED-EB were investigated. A strong anisotropy is found in the material, which can probably be attributed to the pronounced grain growth of the single-phase alloy used as well as the heat conduction in the process. In the tensile specimens taken horizontally, tensile strengths of 245 MPa – 359 MPa are achieved with a very ductile material behavior. However, it should be noted that comparable standardized alloys

such as CuAl8, depending on the product form and heat treatment condition, usually achieve much higher tensile strengths of at least 412 MPa [8]. Recent work by Zykova et al. has enabled tensile strengths of 483 MPa [23], which is close to the lower limit of the material specification of the CuAl9Mn2 material used, by in-situ control of heat input and optimized process control [8].

Accordingly, the achievement and partial surpassing of the material specification in the area of yield strength, tensile strength and at the same time sufficiently good elongation at break in the present work can be assessed as an important step for the processing of high-strength aluminum bronzes by means of DED-EB.

4. Conclusions

The present project focused on an analysis of the suitability of the DED-EB for application on copper alloys, by the example of high-strength aluminum bronze. In the first step, preliminary tests were carried out to identify suitable process parameters with a view to achieving good results for volumetric energy, wetting angle, track geometry and dilution. It was found that the dilution is increased at constant volume energy by increasing the welding speed, but the values with a maximum dilution < 12 % are not problematic for the parameters investigated. The wetting angle decreases sharply with increasing volume energy, resulting in track geometries unsuitable for additive manufacturing. A consideration of the volumetric energy proved to be effective in controlling the process. The stable process range was between 18 J/mm³ and 32 J/mm³ for CuAl8Ni6. After determining suitable regions for welding speed and energy input, the scalability of the buildup process was tested by the parameters beam current and wire feed using the constant volumetric energy approach. In principle, the scalability of the process was found to be good by varying the beam current and wire feed in steps. However, when increasing the deposition rate, the change in the seam profile must be considered, since the track width increases much faster than the track height. The results of the hardness measurements confirm the constant volumetric energy approach used for scaling the process. Despite increasing the application rate by a factor of four, there are no noticeable changes in hardness within the manufactured tracks. The suitability of the identified parameters was demonstrated in the final step by building cylinders and walls from both materials. On these additive test components, an observation of the hardness profile, microstructure, tensile strength and elongation at break was carried out. The mechanical properties show good agreement with the material specification. For the alloy CuAl8Ni6, even higher tensile strengths of approx. 690 MPa could be realized compared to the specified value at the same elongation at fracture with around 18 %. Consideration of the hardness curves across the height of the specimens suggests an approximately equal distribution of material properties over the buildup process. Overall, the DED-EB is shown to be suitable for processing high-strength aluminum bronze with high component quality. Within the stable process range investigated, track widths of 2.6 mm and 8.4 mm and track heights between 1.4 mm and 2.9 mm could be achieved in a single track using filler wire of diameter 1.0 mm. The deposition rates achieved range from 0.6 kg/h - 2.5 kg/h, depending on the parameter settings.

Author Contributions: Conceptualization, J.Raute; methodology, J.Raute; formal analysis, J.Raute; investigation, J.Raute; resources, J.Raute; data curation, J.Raute; writing—original draft preparation, J.Raute; writing—review and editing, M. Biegler and M. Rethmeier.; visualization, J.Raute; supervision, M. Biegler and M. Rethmeier; project administration, J.Raute and M.Biegler; funding acquisition, J.Raute and M.Biegler. All authors have read and agreed to the published version of the manuscript.

Funding: This research was funded by Dobeneck-Technologie-Stiftung, project title: “Prozessevaluierung und Erweiterung der Einsatzmöglichkeiten beim WEBAM von Cu-Werkstoffen“.

Conflicts of Interest: The authors declare no conflict of interest. The funders had no role in the design of the study; in the collection, analyses, or interpretation of data; in the writing of the manuscript; or in the decision to publish the results.

References

1. L. Constantin, Z. Wu, N. Li, L. Fan, J. F. Silvain, Y. F. Lu, "Laser 3D printing of complex copper structures," Additive Manufacturing, vol. 35, pp. 1–22, 2020.
2. P. Yang, X. Guo, D. He, W. Shao, Z. Tan, H. Fu, Z. Zhou, X. Zhang, "Microstructure Twinning and Mechanical Properties of Laser Melted Cu-10Sn Alloy for High Strength and Plasticity," Journal of Materials Engineering and Performance, vol. 31, no. 4, pp. 2624–2632, 2022.
3. G. Mayer, J. Zähr, U. (TUD) Füssel, "Schweißen von Kupfer und Kupferlegierungen," Deutsches Kupferinstitut, 2009.
4. H. Siva Prasad, F. Brueckner, J. Volpp, A. F. H. Kaplan, "Laser metal deposition of copper on diverse metals using green laser sources," International Journal of Advanced Manufacturing Technology, vol. 107, no. 3–4, pp. 1559–1568, 2020.
5. E. Hori, Y. Sato, T. Shibata, K. Tojo, M. Tsukamoto, "Development of SLM process using 200 W blue diode laser for pure copper additive manufacturing of high density structure," Journal of Laser Applications, vol. 33, pp. 1–4, 2021.
6. J. Wang, X. Zhou, J. Li, J. Zhu, M. Zhang, "A comparative study of Cu–15Ni–8Sn alloy prepared by L-DED and L-PBF: Microstructure and properties," Materials Science and Engineering: A, vol. 840, p. 142934, Apr. 2022.
7. C. L. Yao, H. S. Kang, K. Y. Lee, J. G. Zhai, D. S. Shim, "A study on mechanical properties of CuNi2SiCr layered on nickel–aluminum bronze via directed energy deposition," Journal of Materials Research and Technology, vol. 18, pp. 5337–5361, May 2022.
8. Deutsches Kupferinstitut, "Kupfer-Aluminium-Legierungen," 2010.
9. Y. Wang, X. Chen, S. Konovalov, C. Su, A. N. Siddiquee, N. Gangil, "In-situ wire-feed additive manufacturing of Cu-Al alloy by addition of silicon," Applied Surface Science, vol. 487, no. May, pp. 1366–1375, 2019.
10. W. Chen, Y. Chen, T. Zhang, T. Wen, X. Feng, L. Yin, "Effects of Location on the Microstructure and Mechanical Properties of Cu-8Al-2Ni-2Fe-2Mn Alloy Produced Through Wire Arc Additive Manufacturing," Journal of Materials Engineering and Performance, vol. 29, no. 7, pp. 4733–4744, Jul. 2020.
11. C. Guo, T. Kang, S. Wu, M. Ying, W. M. Liu, F. Chen, "Microstructure, mechanical, and corrosion resistance of copper nickel alloy fabricated by wire-arc additive manufacturing," MRS Communications, vol. 11, no. 6, pp. 910–916, 2021.
12. Y. Wang, S. Konovalov, X. Chen, Y. Ivanov, S. Jayalakshmi, R. A. Singh, "Research on Cu-6.6%Al-3.2%Si Alloy by Dual Wire Arc Additive Manufacturing," Journal of Materials Engineering and Performance, no. 2, pp. 1–9, 2021.
13. R. Guschlbauer, F. Osmanlic, C. Körner, "Herausforderungen bei der Additiven Fertigung von Reinkupfer mit dem selektivem Elektronenstrahlschmelzen," METALL, pp. 459–462, 2017.
14. E. Sharabian, M. Leary, D. Fraser, S. Gulizia, "Electron beam powder bed fusion of copper components: a review of mechanical properties and research opportunities," International Journal of Advanced Manufacturing Technology, vol. 122, no. 2, pp. 513–532, 2022.
15. S. Megahed, F. Fischer, M. Nell, J. Forsmark, F. Leonardi, L. Zhu, K. Hameyer, J. H. Schleifenbaum, "Manufacturing of Pure Copper with Electron Beam Melting and the Effect of Thermal and Abrasive Post-Processing on Microstructure and Electric Conductivity," Materials, vol. 16, no. 1, pp. 1–13, 2023.
16. K. N. Kalashnikov, V. E. Rubtsov, N. L. Savchenko, T. A. Kalashnikova, K. S. Osipovich, A. A. Eliseev, A. V. Chumaevskii, "The effect of wire feed geometry on electron beam freeform 3D printing of complex-shaped samples from Ti-6Al-4V alloy," International Journal of Advanced Manufacturing Technology, vol. 105, no. 7–8, pp. 3147–3156, 2019.
17. J. Fuchs, C. Schneider, N. Enzinger, "Wire-based additive manufacturing using an electron beam as heat source," Welding in the World, pp. 267–275, 2018.
18. F. Pixner, F. Warchomicka, P. Peter, A. Steuwer, M. H. Colliander, R. Pederson, N. Enzinger, "Wire-Based Additive Manufacturing of Ti-6Al-4V Using Electron Beam Technique," Materials, pp. 1–23, 2020.
19. D. A. Gurianov, S. V. Fortuna, "Wire-feed electron beam additive manufacturing of nickel-based superalloy: Process stability and structure features," AIP Conference Proceedings, vol. 2310, no. 020120, pp. 1–5, 2020.

20. B. Baufeld, S. Schönfelder, T. Löwer, "Wire Electron Beam Additive Manufacturing at pro-beam," in International Electron Beam Welding Conference, 2021, pp. 93–99.
21. B. Baufeld, "Wire Electron Beam Additive Manufacturing of Copper," pro-beam additive manufacturing GmbH, 2022.
22. E. Khoroshko, A. Filippov, S. Tarasov, N. Shamarin, E. Kolubaev, E. Moskvichev, D. Lychagin, "Study of the Structure and Mechanical Properties of Aluminum Bronze Printed by Electron Beam Additive Manufacturing," Obrabotka Metallov, vol. 22, no. 2, pp. 118–129, 2020.
23. A. P. Zykova, A. O. Panfilov, A. V. Chumaevskii, A. V. Vorontsov, S. Y. Nikonov, E. N. Moskvichev, D. A. Gurianov, N. L. Savchenko, S. Y. Tarasov, E. A. Kolubaev, "Formation of Microstructure and Mechanical Characteristics in Electron Beam Additive Manufacturing of Aluminum Bronze with an In-Situ Adjustment of the Heat Input," Russian Physics Journal, vol. 65, no. 5, pp. 811–817, 2022.
24. Copper Development Association Inc., "Aluminum Bronzes - Overview," 2002. [Online]. Available: https://www.copper.org/resources/properties/microstructure/al_bronzes.html.